



HAL
open science

Lipid nanocapsules maintain full integrity after crossing a human intestinal epithelium model

Emilie Roger, Jean Christophe Gimel, Conor Bensley, Andrey S Klymchenko,
Jean Pierre Benoit

► **To cite this version:**

Emilie Roger, Jean Christophe Gimel, Conor Bensley, Andrey S Klymchenko, Jean Pierre Benoit. Lipid nanocapsules maintain full integrity after crossing a human intestinal epithelium model. *Journal of Controlled Release*, 2017, 253, pp.11-18. 10.1016/j.jconrel.2017.03.005 . hal-03805634

HAL Id: hal-03805634

<https://univ-angers.hal.science/hal-03805634>

Submitted on 2 Nov 2023

HAL is a multi-disciplinary open access archive for the deposit and dissemination of scientific research documents, whether they are published or not. The documents may come from teaching and research institutions in France or abroad, or from public or private research centers.

L'archive ouverte pluridisciplinaire **HAL**, est destinée au dépôt et à la diffusion de documents scientifiques de niveau recherche, publiés ou non, émanant des établissements d'enseignement et de recherche français ou étrangers, des laboratoires publics ou privés.

Accepted Manuscript

Lipid nanocapsules maintain full integrity after crossing a human intestinal epithelium model

Emilie Roger, Jean-Christophe Gimel, Conor Bensley, Andrey S. Klymchenko, Jean-Pierre Benoit



PII: S0168-3659(17)30109-8
DOI: doi: [10.1016/j.jconrel.2017.03.005](https://doi.org/10.1016/j.jconrel.2017.03.005)
Reference: COREL 8690

To appear in: *Journal of Controlled Release*

Received date: 15 December 2016
Revised date: 27 February 2017
Accepted date: 3 March 2017

Please cite this article as: Emilie Roger, Jean-Christophe Gimel, Conor Bensley, Andrey S. Klymchenko, Jean-Pierre Benoit , Lipid nanocapsules maintain full integrity after crossing a human intestinal epithelium model. The address for the corresponding author was captured as affiliation for all authors. Please check if appropriate. Corel(2017), doi: [10.1016/j.jconrel.2017.03.005](https://doi.org/10.1016/j.jconrel.2017.03.005)

This is a PDF file of an unedited manuscript that has been accepted for publication. As a service to our customers we are providing this early version of the manuscript. The manuscript will undergo copyediting, typesetting, and review of the resulting proof before it is published in its final form. Please note that during the production process errors may be discovered which could affect the content, and all legal disclaimers that apply to the journal pertain.

Lipid nanocapsules maintain full integrity after crossing a human intestinal epithelium model

Emilie Roger^{*,a}, Jean-Christophe Gimel^a, Conor Bensley^a, Andrey S. Klymchenko^b, Jean-Pierre Benoit^a

^a MINT, UNIV Angers, INSERM 1066, CNRS 6021, Université Bretagne Loire, MINT' IBS-CHU, 4 rue Larrey, 49933 Angers, France.

^bUniversity of Strasbourg, CNRS UMR7213, Laboratoire de Biophotonique et Pharmacologie, 74 route du Rhin, 67401 Illkirch Cedex, France

* corresponding author's: emilie.roger@univ-angers.fr

ABSTRACT

Lipid nanocapsules (LNCs) have demonstrated great potential for the oral delivery of drugs having very limited oral bioavailability (BCS class II, III and IV molecules). It has been shown previously that orally-administered LNCs can permeate through mucus, increase drug absorption by the epithelial tissue, and finally, increase drug bioavailability. However, even if transport mechanisms through mucus and the intestinal barrier have already been clarified, the preservation of particle integrity is still not known. The aim of the present work is to study *in vitro* the fate of LNCs after their transportation across an intestinal epithelium model (Caco-2 cell model). For this, two complementary techniques were employed: Förster Resonance Energy Transfer (FRET) and Nanoparticle Tracking Analysis (NTA). Results showed, after 2 hours, the presence of nanoparticles in the basolateral side of the cell layer and a measurable FRET signal. This provides very good evidence for the transcellular intact crossing of the nanocarriers.

KEYWORDS

Nanocapsules, Caco-2, intestinal transport, FRET, integrity

1. Introduction

The oral route is the most common route for drug delivery. However, oral bioavailability is influenced by drug solubility and permeability. For drugs belonging to the Biopharmaceutics Classification System class II (high permeability, low solubility), class III (low permeability, high solubility), and class IV (low permeability, low solubility) [1], drug encapsulation in nanocarriers provides an alternative solution to enhance bioavailability. Indeed, knowledge of the relationship between physico-chemical characteristics of nanocarriers (size and nature of wall material, surface charge, ligands...) and the gastrointestinal physiology (acidic pH, digestive enzymes of gastrointestinal media, mucus and intestinal barrier), allowed drug bioavailability [2] to be enhanced. In the literature, various nanocarriers (liposomes, micelles, polymeric and lipid-based nanoparticles) are described for the oral delivery of chemotherapeutics, proteins, peptides, vaccines, etc. [3]

Lipid nanocapsules, developed by our group, have also proved to be very interesting for oral administration [4]. These nanoparticles have a size range from 20 to 100nm and are prepared by a well-known low-energy emulsification process: the phase-inversion temperature method [5–7]. They have already shown promising properties for the oral delivery of paclitaxel [8,9], Sn38 [10], fondaparinux [11] and miltefosine [12]. Indeed, LNCs have demonstrated *in vitro* stability in simulated gastrointestinal media[13]. They have also shown their stability and diffusion in intestinal mucus [14]. Furthermore, in a previous study by Roger *et al.* [15], it was shown that LNCs were taken up by Caco-2 cells mainly via active endocytic and more particularly via clathrin-dependent and caveolae-dependent transport mechanisms; this active transport was not size-dependent. Comparing the incubation of paclitaxel-LNCs at 4°C and 37°C, an important decrease of paclitaxel permeability at 4°C was observed (more than 10-fold for the larger LNCs)

and so, very few passive transport was evidenced. Moreover, tight junctions were not disrupted by LNCs and consequently paracellular transport was not possible. Finally, using transmission electron microscopy (TEM), nano-objects were observed on the basolateral side of the Caco-2 cell monolayers when LNCs were applied on the apical side, which probably allow the formulation of a transcytosis hypothesis [15]. Additionally, these nanocarriers have demonstrated a direct effect of P-gp on their endocytosis [16]. In view of these results, LNCs have the ability to enhance the bioavailability of class II and IV drugs [17].

Besides, another challenge of drug delivery via the oral route is to target pharmacological receptors after absorption, like nanocarriers injected via the intravenous route (I.V.). For this purpose, it is important to design nanocarriers that are able to be absorbed while keeping their integrity, and thus able to behave as circulating nanocarriers. Nevertheless, even if the mechanisms of transporting nanocarriers through the intestinal barrier have been well characterised, the fate of these nanocarriers after oral delivery is still unknown [3]. This lack can be explained by the difficulty to find relevant methods to confirm the real integrity of the carrier after absorption [18]. Indeed, many physico-chemical characterisation techniques such as dynamic light scattering (size and charge analysis), microscopy (TEM, AFM, confocal) and spectroscopy (IR, UV, FTIR, NMR) characterise the overall carrier structure or its individual components but not its integrity -*i.e.* is the cargo still inside the carrier? In this way, new tools are needed to determine how nanocarriers are absorbed and eliminated.

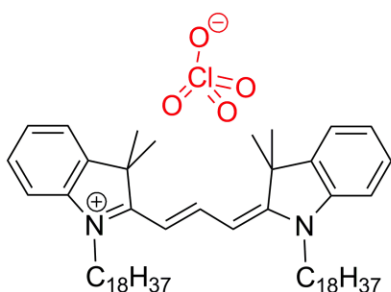
FRET is the most common fluorescence spectroscopy technique used to monitor the proximity at the nanoscale level [18]. It is based on the interactions between spatially-close (2 to 10 nm) donor and acceptor dye molecules. FRET occurs when the emission spectrum of the donor overlaps with the excitation spectrum of the acceptor. The excitation energy of the donor is

transferred to the acceptor whose subsequent emission can be detected. FRET is highly sensitive to donor-acceptor distances and consequently it indicates a preserved nanoscale environment. This technique is widely used to study biological phenomena such as interactions between proteins or proteins and nucleic acids, conformational changes, lipid membrane dynamics, host-pathogenic interactions, etc. [19]. More recently, FRET has been used to study the integrity of nanocarriers *in vitro* in different media, after cell internalisation, or *in vivo* after I.V. administration [20–29]. Importantly, it enables quantification of nanocarrier integrity *in vitro* and *in vivo* [20]. Only 3 studies involving FRET and oral administration have been reported. Firstly, Groo *et al.* [14] demonstrated the integrity of LNCs, using 1,1'-dioctadecyl-3,3,3',3'-tetramethylindocarbocyanine perchlorate (DiI) and 1,1'-dioctadecyl-3,3,3',3'-tetramethylindodicarbocyanine perchlorate (DiD) as FRET pairs, after contact with mucus. Lu *et al.* [30] used fluorescein isothiocyanate (FITC) and Rhodamine B pairs to monitor the assembly of nanocomplexes while pH evolves in the intestine. More recently, Li *et al.* [31] developed a FRET assay with DiO and DiI pairs to evaluate nanostructured lipid carrier (NLC) structural integrity in cell uptake; they observed a FRET signal in Caco-2 cells, and they speculated that NLCs could maintain their structural integrity after crossing intestinal cells, but they did not prove it. To our knowledge, no published work has clearly highlighted the integrity of nanocarriers after their transport through the intestinal barrier.

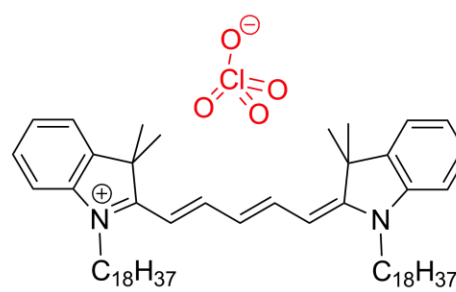
In order to use the FRET technique to study nanocarrier transport across enterocytes with a Transwell[®] set-up, it is important firstly to reach an efficient encapsulation load for both dyes leading to acceptable FRET efficiency [32] and, secondly, to measure with high sensitivity the FRET signal, since a high level of dilution is expected in the basolateral compartment. Moreover, to avoid the immediate partitioning of dye from the carrier to subcellular lipid

compartments, which could decrease FRET efficiency even if nanocarriers are still intact; it is crucial to achieve very stable dye encapsulation with no significant leakage. According to Bastiat *et al.* [33], loading lipophilic carbocyanine dyes (DiO, DiI and DiD) is recommended since, unlike other dyes, they remain inside the nanocapsules in the presence of lipid acceptor compartments.

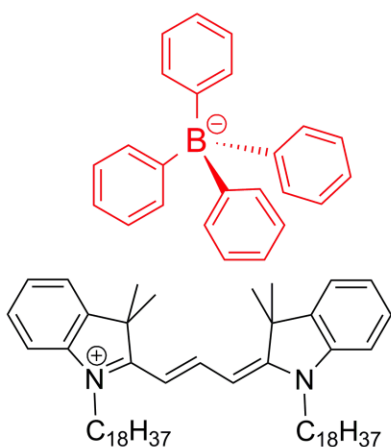
Furthermore, to increase the loading of carbocyanine dyes into the lipidic core of the LNCs and to obtain a significant FRET signal, a new concept of counterion-based dye was introduced by Kilin *et al.* [34]. They substituted the perchlorate counterion for the bulky and highly hydrophobic tetraphenyl borate (TPB) which improves dye solubility in oil and consequently the dye loading capacity (Figure 1).



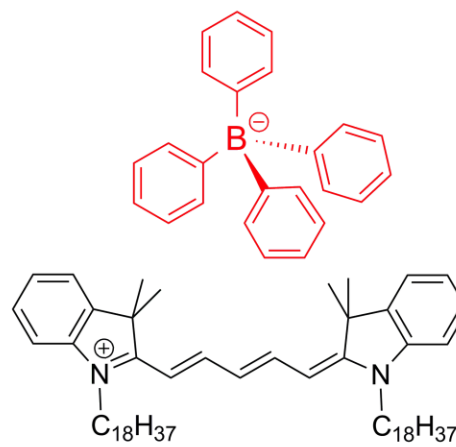
DiI-perchlorate



DiD-perchlorate



DiI-TPB



DiD-TPB

Figure 1. Chemical structures of DiI and DiD dyes with perchlorate and tetraphenylborate (TPB) counterions.

In this context, we encapsulated two lipophilic cyanine dyes (DiD and DiI) bearing TPB counterions inside 50 nm LNCs. We optimised dye loading to achieve an efficient FRET signal. Then, the transport of the obtained ultrabright FRET-loaded LNCs was studied with a well-established intestinal epithelium model (Caco-2 cells) [35,36]. To complete this approach, NTA was also performed to measure the size distribution of nanoparticles and their concentration. The objective of the present study is to investigate the fate of LNCs after crossing the intestinal barrier, focusing on nanoparticle integrity.

2. Materials and Methods

Materials

All the chemicals and solvents for synthesis were from Sigma-Aldrich (Saint-Quentin Fallavier, France). Captex[®] 8000 (tricaprylin) was a gift from Abitec Corp. (Columbus, Ohio, USA). Lipoid[®] S75-3 (soybean lecithin at 70% of phosphatidylcholine and 10% of phosphatidylethanolamine) and Kolliphor[®] HS15 (mixture of free polyethylene glycol 660 and polyethylene glycol 660 hydroxystearate) were purchased from Lipoid GmbH (Ludwigshafen, Germany) and BASF (Ludwigshafen, Germany), respectively. NaCl was purchased from Prolabo VWR International (Fontenay-sous-Bois, France). Ultrapure water was obtained from a Milli-Q[®] Advantage A10 System (Merck Millipore, Darmstadt, Germany). Culture reagents were obtained from Sigma (St.Louis, USA) and Lonza (Verviers, Belgium).

Preparation of DiI-TPB and DiD-TPB

DiI-TPB was synthesized as described elsewhere [34]. To synthesize DiD-TPB, 100 mg of 1,1'-Diocadecyl-3,3,3',3'-Tetramethylindodicarbocyanine perchlorate (DiD, Life Technologies,

USA) was mixed with 0.71 g (20 mol eq.) of sodium tetraphenylborate in ethyl acetate, which dissolved both salts easily. The formation of the desired salt was confirmed by thin-layer chromatography, where the product moved much faster than the starting DiD perchlorate (dichloromethane/methanol, 95/5). After solvent evaporation, the product (DiD-TPB) was purified by column chromatography (dichloromethane/methanol, 95/5).

Formulation and characterisation of lipid nanocapsules (LNCs)

LNC formulation was based on a phase-inversion process and has been thoroughly described [5,6]. Briefly, the fluorescent dyes were solubilised in Captex[®] 8000. Then, 150 mg of Captex[®] 8000 (oil phase), 225.0 mg of water, 9.1 mg of NaCl (aqueous phase), 8.4 mg of Lipoid[®] S75-3 and 125 mg of Kolliphor[®] HS15 (surfactants) were precisely weighed. After this, three cycles of heating and cooling between 70 and 90°C were carried out and the suspension of LNCs was obtained by adding 625 µL of water. LNC suspensions were filtered (0.22 µm) before use.

Formulation and characterisation of nanoemulsions (NEs)

Nanoemulsions were prepared by spontaneous nano-emulsification. The fluorescent dyes were solubilised in Captex[®] 8000. Then, 105 mg of Captex[®] 8000 and 160 mg of Kolliphor[®] HS15 and 8.4 mg of Lipoid[®] S75-3 were weighed and homogenised under magnetic stirring at 90°C. Nano-emulsions were formed by adding 860 µL of cold water.

Nanoparticle Tracking Analysis (NTA) measurements

The concentration and the size distribution of particles were determined using a NS300 NanoSight (Malvern Instrument, Worcesterchire, UK) with a low-volume flow cell plate and a 405 nm laser. The nanoparticle suspensions were put directly into the chamber using a 1 mL syringe installed on a syringe pump. We used the NTA analytical software, version 3.2, to analyse video images. The measurements were made at room temperature, and each video

sequence was captured over 60 s. Each analysis was replicated five times for each sample. Concentrations inferior to 5 particles/frame were considered as unreliable, and corresponding samples were considered as being without particles. LNC and NE suspensions were diluted in ultrapure water by factor 6,000,000 (v/v) before analysis. Apical and basolateral media were diluted in ultrapure water by factor 50,000 and 10 (v/v), respectively, before analysis. We haven't done measurements using the fluorescence mode of the NTA as the measured fluorescence of a NP varies depending on its position with respect to the focal plane.

Caco-2 cell culture: model of gastrointestinal barrier

The human colon adenocarcinoma cell line (Caco-2) was obtained from the American Type Culture Collection (Manassas, USA) and used between passages 26 and 30. Cells were cultured in Dulbecco's modified Eagle medium (D-MEM, high glucose) supplemented with 15% (v/v) foetal bovine serum, 1% (v/v) non-essential amino acids, 1% (v/v) sodium pyruvate, and 1% antibiotic solution (1·10⁴ UI/mL penicillin, 10mg/mL streptomycin, 25 µg/mL amphotericin B) in a humidified incubator 5% CO₂/95% air atmosphere at 37°C. Cells were plated on a 75 cm² flask at a density of 1·10⁶ cells/flask and were then harvested at 80% confluence with trypsin-EDTA and seeded onto polycarbonate membrane filters (0.4 µm pore size, 1.12 cm² growth area) inside Transwell[®] cell culture chambers (Corning Costar, Cambridge, MA) at a density of 0.1·10⁶ cells/insert. The culture medium (0.5 mL per insert and 1.5 mL per well) was replaced every two days for the first two weeks and everyday thereafter. After 21 days in culture, cell monolayers were used for the following assays. Before experiments, cell monolayers were washed twice with Hank's buffered salt solution (HBSS) for 15 min at 37 °C. The transepithelial electrical resistance (TEER) of monolayers was checked before and after each experiment by using a Millicell[®]-ER-2

system (Millipore Corporation, Billerica, MA). Only cell monolayers with TEER values over $250 \Omega \cdot \text{cm}^2$ were used.

Nanoparticle transport across Caco-2

The integrity of lipid nanocarriers was estimated using Förster Resonance Energy transfer (FRET) between two encapsulated dyes, 0.5% of DiI-TPB (with respect to Captex[®] 8000) as energy donor and 0.5% of DiD-TPB as energy acceptor were used. The transports of NEs, LNCs and HBSS (control) were studied in the apical to basolateral direction on Caco-2 cells in quadruplicate. Nanoparticle (LNC and NE) suspensions were diluted 100 times in HBSS and 1% of HEPES from the original formulation and were applied on all the apical side. Experiments were started by adding 0.5 mL of test solution at the apical side and 1.5 mL of HBSS / HEPES at the basolateral side. After 2 h of incubation at 37°C, samples were taken from apical and basolateral sides (n=4) and the nanocarrier integrity was determined by FRET measurements coupled to NTA.

Fluorescence spectroscopy

Fluorescence spectra were recorded on a FluoroMax[®]-4 spectrophotometer (HORIBA Jobin Yvon Inc., New Jersey, USA). Fluorescence emission spectra were recorded at room temperature with 520 nm excitation wavelengths, with an excitation slit width of 3 nm, an emission slit width of 2 nm and an integration time of 0.5 s. Emission spectra were collected from 530 to 720 nm with a 1 nm increment. They were corrected for the lamp source fluctuations and the wavelength-dependent response of the detector.

The semi-quantitative parameter of FRET efficiency was calculated according to the following equation $PR=A/(A+D)$, where A and D are the maximum of fluorescence intensity of the acceptor (674 nm) and donor (570 nm), respectively.

3. Results and discussion

As seen previously, the LNC platform represents one type of nanoparticle with promising use for oral delivery. They are formulated with Generally Recognized as Safe (GRAS) excipients by a phase-inversion temperature (PIT) process, a low-energy nano-emulsification method[6]. LNCs are composed of an oily core (Captex[®]8000: a medium-chain triglyceride) surrounded by a mixed layer of lecithin (Lipoid[®]S-75) and a PEGylated surfactant (Kolliphor[®]HS15)[6]. Different *in vitro* and *in vivo* experiments have demonstrated the ability of LNCs to diffuse across mucus and to enhance drug intestinal permeability as well as to improve paclitaxel bioavailability [9,15,17]. Nevertheless, a better understanding of the fate of these LNCs for oral drug delivery should be investigated in order to determine how the carriers are absorbed before planning thorough biodistribution studies.

As a comparison, we also tested nanoemulsions (NEs), a system close to LNCs. They are also formulated by a low-energy method with the same excipients but are obtained by a spontaneous emulsification mechanism [37]. Compared to LNCs, NEs use a different formulation pathway that never goes through the microemulsion step as with the PIT method [38,39]. Both systems were applied on the apical side of a Caco-2 cell monolayer and NEs were considered as a control. In the following we mainly focused on LNC behaviour.

The use of FRET to assess LNC integrity has been successfully employed for *in vitro* stability in mucus [14] and in plasma [22] as well as for *in vivo* biodistribution after intravenous administration [22,27]. Nevertheless, no work to date has demonstrated the potential of LNCs to cross the intestinal barrier in an intact form; only the presence of nano-objects on the basolateral side has been evidenced by TEM when LNCs were applied on the apical side of enterocytes [15], but no proof of integrity was established. Consequently, in order to achieve this, it is important to

have a highly-efficient FRET signal combined with a high-detection capability of the fluorescence emission. For this, dyes had to be closely confined and a high dye loading was requested without any dye precipitation or release. Simonsson *et al.* [40] studied the potential transfer of various lipophilic dyes from the LNC core to favourable lipidic environments present in the cell. They demonstrated *in vitro* that no transfer of lipophilic carbocyanine dyes (DiI, DiD, DiO) occurred whereas a rapid transfer of Nile Red was observed from LNCs to cells. Consequently, carbocyanine dyes are more appropriate for FRET use. More recently, Kilin *et al.* [34] introduced the substitution of the perchlorate counterion by a bulky and hydrophobic tetraphenylborate one to increase dye solubility in oil. Based on these works, we formulated various LNCs with DiI-TPB and/or DiD-TPB that showed solubility in Captex[®] above 3 % w/w. Firstly, single dye-loaded LNCs were formulated and the fluorescent spectra were measured. Figure 2 presents excitation and emission spectra of both individually-loaded dyes. An overlay of the emission spectrum of DiI-TPB with the excitation spectrum of DiD-TPB was observed (see the hatched patterns in Figure 2a). Accordingly, a FRET signal could be expected with DiI-TPB as a donor and DiD-TPB as an acceptor. The maximum of the excitation spectrum of DiI is 548 nm but, in order to minimise DiD-TPB direct excitation, a wavelength of 520 nm was preferred as the excitation level for the FRET signal, *i.e.* using 520 nm instead of 548 nm reduced by a factor of 4 the emission intensity of DiD-TPB from direct excitation (supplementary Figure 1S). Nevertheless, even with excitation at 520 nm, a low-intensity emission peak of DiD-TPB LNCs at 674 nm was still noticeable (see the red-dashed line in Figure 3) as well as a residual contribution of the donor itself (see the blue-dashed line in Figure 3). The emission spectrum of a mixture of DiI-TPB LNCs and DiD-TPB LNCs appeared as a simple sum of the individual emission spectra (see the full-black line in Figure 3), which is a relatively low contribution level

of the acceptor (DiD-TPB) peak at 674 nm. In contrast, when DiI-TPB and DiD-TPB were both encapsulated inside the same LNCs, the so-called FRET-LNCs, a significant FRET signal occurred: a significant increase of the acceptor (DiD-TPB) peak at 674 nm was observed together with a decrease at 568 nm of the donor (DiI-TPB) (see the full-red line in Figure 3). This phenomenon was specific of a fluorescent energy transfer between the two dyes due to their close confinement in the LNCs. Fluorescence spectra of FRET-LNCs, with an increasing amount of DiI-TPB and DiD-TPB, are represented in Figure 4A. As the concentration of both dyes increased (in a mass ratio 1:1), an increase in the acceptor emission band was clearly seen, whereas the donor's band was saturated. This could be formally highlighted by calculating the relative FRET efficiency, also called the proximity ratio (PR), that characterises the efficacy of the transfer and that is closely related to the dye proximity [19,32,41]. It was calculated as the ratio of the acceptor intensity at the peak (A) to the total intensity (A+D) where D was the intensity at the donor peak, upon donor excitation (at 520 nm): $PR=A/(A+D)$. This value is reported in the inset of Figure 4A with various dye concentrations from 0.1% to 0.5% w/w of Captex[®]. As expected, the most efficient PR was obtained for the highest concentration tested *i.e.* 0.5%. But as the addition of carbocyanine dyes could modify the LNC structure and its zeta potential [14], 0.5% w/w corresponded to a good compromise between a good brightness level and no significant change in the zeta potential (a weakly-negative zeta potential was obtained corresponding to blank LNC values [15]). Moreover, the FRET signal was disrupted when the LNCs were destroyed in organic solvents (Methanol/THF, DMSO, and dioxane) [20,22]. The donor fluorescence was no longer transferred to the acceptor and an emission spectrum close to that of an LNC mixture was recovered (Figure 4B), as well as small shifts in peak positions due

to solvent changes. The resulting values of PR collapse from 0.72 to below 0.22 making PR a reliable indicator of LNC integrity.

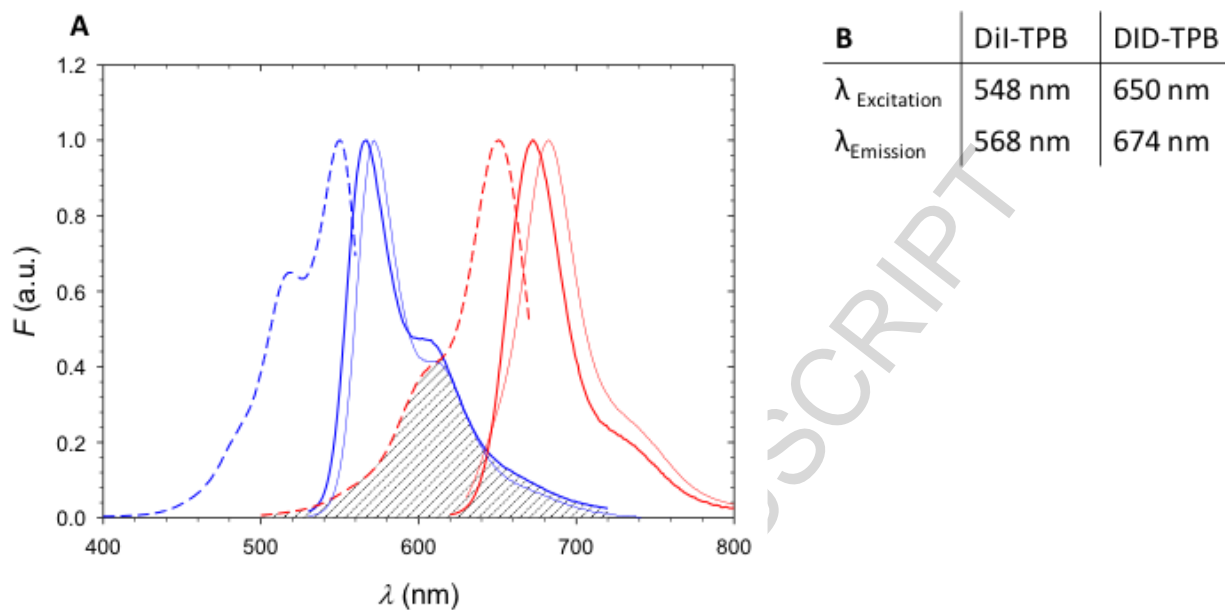


Figure 2. A) Excitation spectra and emission spectra of dye-loaded LNCs (0.5% w/w of Captex[®]). The dashed-blue line (DiI-TPB) and dashed-red line (DiD-TPB) are excitation spectra recorded at $\lambda_{\text{em}}=565$ nm, and $\lambda_{\text{em}}=676$ nm, respectively. The full-blue line (DiI-TPB) and full-red line (DiD-TPB) are emission spectra obtained at $\lambda_{\text{ex}}=520$ nm, and $\lambda_{\text{ex}}=610$ nm, respectively. The cross-region of LNCs DiI-TPB emission and LNCs DiD-TPB excitation is indicated by hatched patterns. For comparison, thin-full lines show emission spectra of DiI-TPB (blue) and DiD-TPB (red) solubilized in pure Captex[®]. All spectra have been normalized to 1 at their maximum value. B) Maximum values of λ_{ex} and λ_{em} of dye-loaded LNCs. (spectra are recorded once due the qualitative character of this measurement)

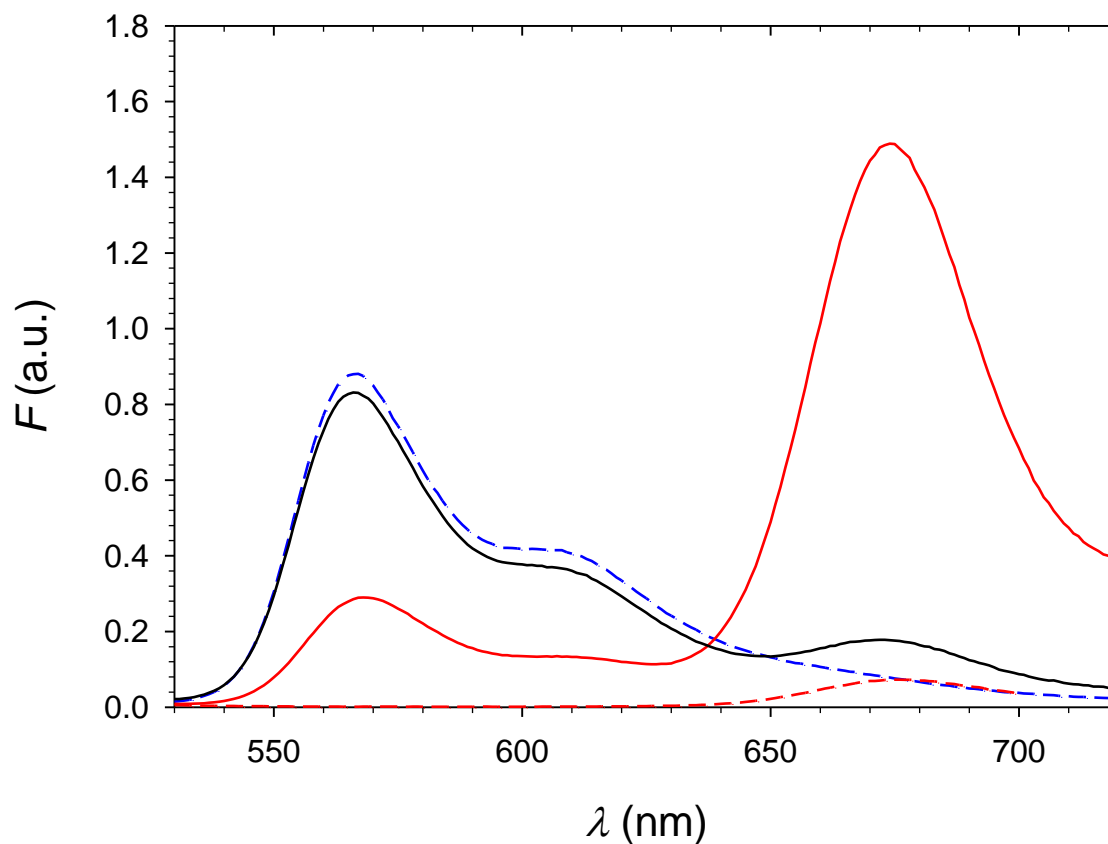


Figure 3. Emission spectra of dye-loaded LNCs. The dashed-blue line: LNCs loaded with DiI-TPB 0.5% w/w, the dashed-red line: LNCs loaded with DiD-TPB 0.5% w/w, the full black line: a mixture of DiI-TPB LNCs and DiD-TPB LNCs both at 0.5% w/w dye-loading, and the full-red line: FRET-LNCs loaded with 0.5% w/w DiI-TPB and DiD-TPB. All spectra have been recorded using $\lambda_{\text{ex}} = 520$ nm, with the same fluorimeter settings and the same 1,000-fold dilution of LNCs in water. The mixture solution contains twice the amount of LNCs to maintain the same concentration of dye per unit of volume in the solution.

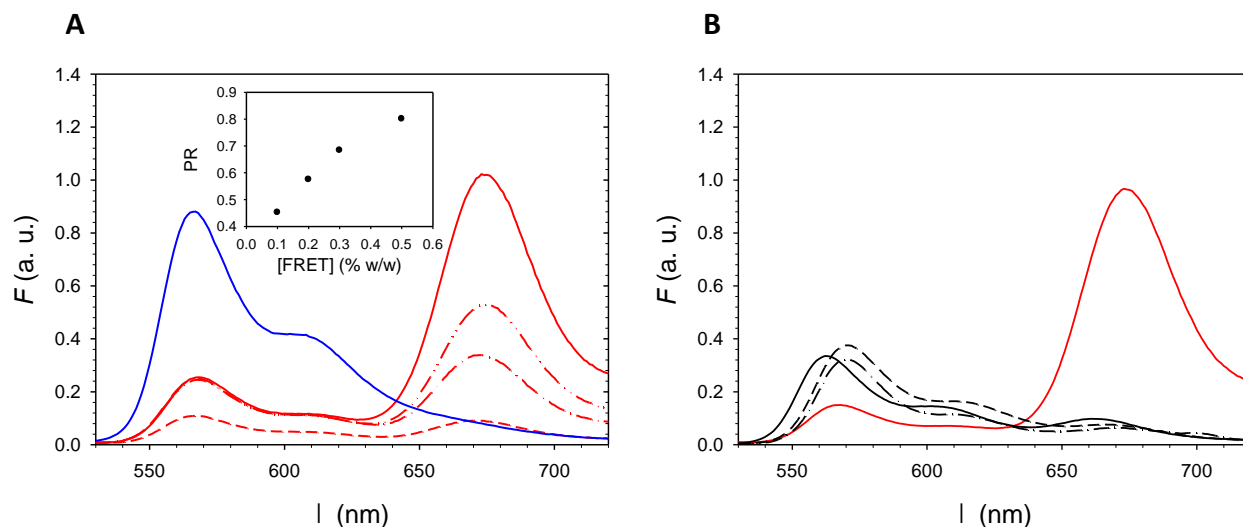


Figure 4. A) Emission spectra of FRET-loaded LNCs for various concentrations of FRET pairs in % w/w of Captex[®]. The dashed-red line: 0.1% w/w, the dashed-dot red line: 0.2% w/w, the dashed-dot-dot line: 0.3% w/w and the full-red line: 0.5% w/w. In comparison, the full-blue line shows the emission spectra of LNCs loaded with DiI-TPB at 0.5% w/w of Captex[®]. All spectra were recorded using $\lambda_{\text{ex}} = 520$ nm, the same fluorimeter settings and the same 1,000-fold dilution of LNCs in water. The inset of A) shows the evolution of the proximity ratio (PR) as a function of the FRET pair concentration (% w/w of Captex[®]). B) Emission spectra of FRET LNCs after a 1,000-fold dilution in various solvents: (full-red line) pure water, (full-black line) methanol/THF (98:2 v/v) mixture, (dashed-black line) DMSO, and (dashed, dotted-black line) Dioxane. All spectra have been recorded using $\lambda_{\text{ex}} = 520$ nm and the same fluorimeter settings.

Afterwards, the LNCs were characterised in terms of size distribution and particle concentration by a nanoparticle tracking technique (NTA). Indeed, due to the excitation spectrum of DiI-TPB, the dynamic light scattering (DLS) method with a laser source at 633 nm could not be used to measure particle size of FRET-LNCs as the resulting emitted light would mostly result from

fluorescence and only a very little from elastic scattering. NTA is a large field optical microscopy technique that gives a direct measurement of individual nanoparticle trajectories in a low volume flow cell illuminated by a laser. Of course, nanoparticle size cannot directly be resolved but its trajectory is recorded and a diffusion coefficient, thus a hydrodynamic diameter, is extracted from each track. This provides information about the number particle size distribution and the particle concentration. This technique has also been used to study the time-dependent effect of biological conditions on nanoparticles [18]. We found a very narrow size distribution of FRET-LNCs with a number average diameter of 55.8 nm (supplementary Figure 2S). The measured concentration was around $1.2 \cdot 10^{15}$ particles/ml.

Figure 2 displays emission spectra of DiI-TPB and DiD-TPB inside LNCs and in pure Captex[®] (the oil component of the LNC core). For both dyes, a slight red shift of their maximum intensity emission (from 568 nm to 572 nm for DiI-TPB, and from 674 nm to 682 nm for DiD-TPB) was noticed in pure Captex[®]. This was characteristic of a change in the dye environment. Therefore, it can be assumed that, in LNCs, dyes were also localised at the core/shell interface and not only in the bulk of the oily core. Finally, as we did the counterion substitution, we had to check that dye-TPB encapsulated inside LNCs behaved like perchlorate ones, and could not partition with another lipidic compartment-like cell membranes [27] which could lead to a FRET signal loss even if the LNCs stayed intact. For this, we investigated the encapsulation stability of dye-loaded LNCs after mixing them with pure Captex[®] oil. No leakage phenomenon was evidenced; FRET efficiency was preserved as well as the size of LNCs even if a small particle concentration decrease was observed (Table 1). This lipid transfer experiment was described by Bastiat *et al.* [33] and authors explained the absence of leakage of lipophilic carbocyanines by their highly hydrophobic stearyl chain. The presence of TPB counterions rendered carbocyanine dyes even

more lipophilic. Thus, FRET-LNCs exhibited relevant properties to assess their integrity. Finally, a FRET-LNC suspension at 0.5wt % of each dye, at a concentration of $0.9 \cdot 10^{15}$ particles/mL, was diluted in water and a fluorescence spectrum was measured for each dilution. As represented in Figure 5, peak fluorescence intensities D (at 568 nm) and A (674 nm) were plotted as a function of the LNC concentration. Both curves were fitted on a double logarithmic scale with a linear function $D = 10^{-6.644} C_{LNC}$ for the donor and $A = 10^{-6.237} C_{LNC}$ for the acceptor (see both straight lines in Figure 5). Based on these calibration curves, fluorescence intensities at 568 nm and 674 nm obtained in the following could be correlated to a concentration of particles. Moreover, for each dilution a proximity ratio (PR) was determined and a value of 0.718 ± 0.117 ($n=21$ dilutions, average $\pm S.D$) was obtained whatever the concentration. A similar calibration curve in terms of Captex[®] concentration was obtained with NEs (supplementary Figure 3S) but with a PR value of 0.512 ± 0.033 ($n=19$ dilutions, average $\pm S.D$) and a size distribution much more polydispersed (supplementary Figure 2S). This large size distribution prevented the establishment of a relevant calibration curve expressed in terms of nanoparticle concentration.

Table 1: FRET efficiency and particle tracking analysis of LNCs during the lipid transfer experiment.

	<i>Proximity Ratio</i>	<i>number average Size (nm)</i>	<i>Concentration of particles (particles/ml)</i>
<i>Before the lipid transfer experiment</i>	0.783	55.8	$1.2 \cdot 10^{15}$
<i>After the lipid transfer experiment</i>	0.781	60.6	$0.8 \cdot 10^{15}$

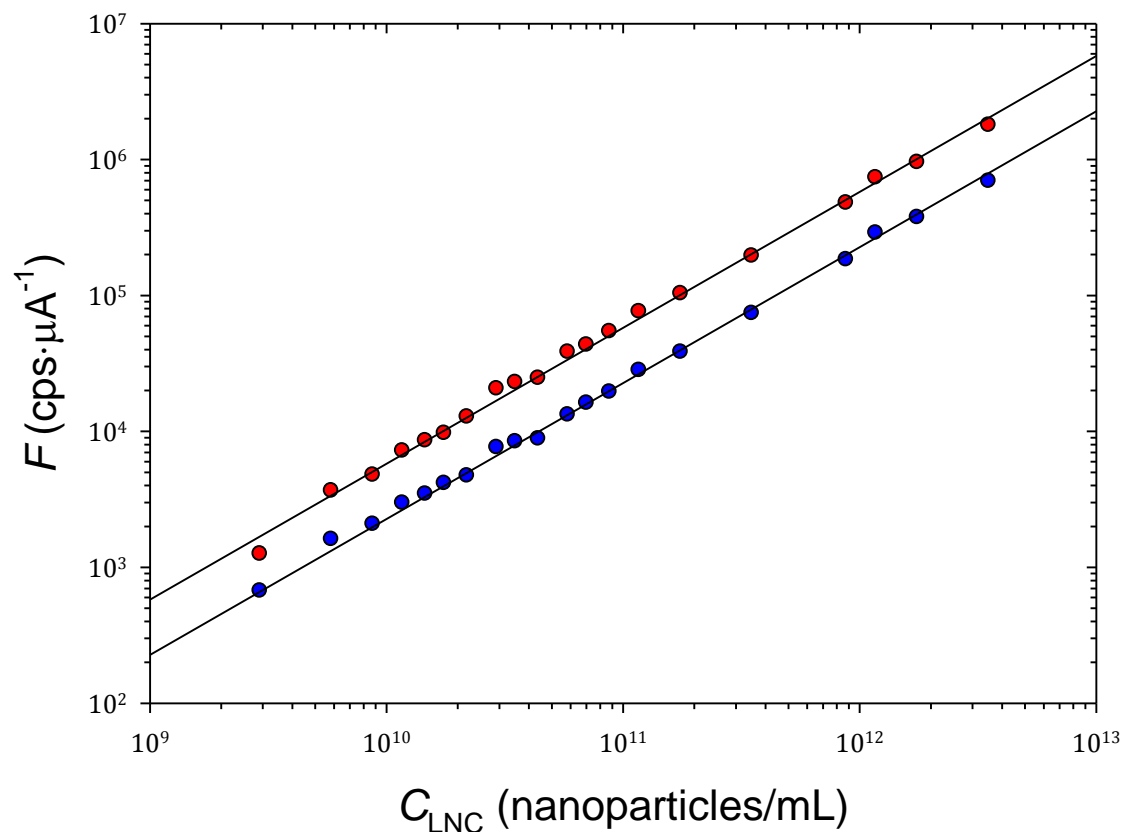


Figure 5. Evolution of the peak fluorescence intensities of the donor (blue circles, $\lambda = 568$ nm) and the acceptor (red circles, $\lambda = 674$ nm), with $\lambda_{\text{ex}} = 520$ nm, as a function of the LNC-FRET concentration. Straight lines represent fits to a function of the form $F = k \cdot C_{\text{LNC}}$. The fitting procedure was performed on logarithmic scales.

To carry out quantitative particle analysis on the basolateral side of the Caco-2 cell monolayer, the fluorescence spectrum at $\lambda_{\text{ex}} = 520$ nm was measured. Firstly, the PR was checked for a qualitative measurement of overall LNC integrity, then the concentration of intact particles was estimated with the equations given above and finally compared with the concentration given by NTA. It has to be noted that nanoparticles detected by the NTA technique were not necessarily

LNCs and could result from the metabolic activity of Caco2 cells. Only the combination of both techniques allowed us to state that intact LNCs were present in the basolateral compartment.

Before performing transport experiments in Transwell[®] systems, the stability of FRET-LNCs and FRET-NEs was assessed by incubating them at a 100-fold dilution in HBSS at 37°C, conditions used for *in vitro* studies. Firstly, no significant change was observed in the proximity ratio value nor in the particle size after 2 hours, the incubation time used for transport experiments (Table 2). Moreover, no variation in the concentration of particles calculated either with the fluorescence calibration curve at 674 nm or determined directly by NTA was observed. Consequently, one could conclude that both FRET-LNCs and FRET-NEs had very good stability at 37°C and could be used safely for *in vitro* experiments. Even so, the concentration of FRET-LNC particles obtained by fluorescence calculation or by NTA showed a slight difference ($0.6 \cdot 10^{15}$ particles/mL *versus* $0.9 \cdot 10^{15}$ particles/mL, respectively at the initial time for LNC). This difference was still present after 2 hours of incubation and could be explained by the presence of dust particles in the HBSS medium or in the water used for the dilutions needed to perform NTA (even though HBSS and dilution water were filtrated through a 0.22 μ m filter). These particles were counted by the NTA technique but did not contribute to the fluorescence signal which explains the discrepancy observed.

Table 2. Stability of FRET-LNCs and FRET-NEs in biological conditions: proximity ratio, concentration of particles (calculated with the equation obtained at 674 nm and determined by NTA) and size of particles (*N.A* for not applicable).

	<i>Time (h)</i>	<i>Proximity Ratio</i>	<i>Concentration of particles (particles/mL)</i>		<i>Number average Size (nm)</i>
			<i>Calculated by fluorescence at 674 nm</i>	<i>Determined by NTA</i>	
LNCs	0	0.737	$0.6 \cdot 10^{15}$	$0.9 \cdot 10^{15}$	67.1
	2	0.735	$0.6 \cdot 10^{15}$	$0.8 \cdot 10^{15}$	72.8
NEs	0	0.564	<i>N.A</i>	$0.5 \cdot 10^{15}$	83.0
	2	0.564	<i>N.A</i>	$0.5 \cdot 10^{15}$	75.1

The *in vitro* transport across Caco-2 cells was then performed in quadruplicate to take into account the variability of the biological activity from one well to another one. The basolateral medium was analysed after 2 hours of incubation with FRET-LNCs, FRET-NEs or HBSS (controls) in the apical side. TEER values were checked before and after the incubation; no significant TEER decrease and typical values between 300 and 450 $\Omega \cdot \text{cm}^2$ were obtained confirming that no paracellular transport was possible. As summarized in Table 3 and Figures 6 and 7, in control HBSS no particles were observed on the apical side nor on the basolateral side. With control FRET-NE particles, a number average size above 87 nm were found with a Proximity Ratio value of 0.549 in the apical side, but neither particles nor a FRET signal were detected on the basolateral side. This result suggested an absence of the transport of intact NEs across Caco-2 cells. However, using FRET-LNCs particles, fluorescence spectra performed in the basolateral side showed clearly a FRET signal with an average PR value close to 0.75 even if

absolute peak intensity varies from 1 to 6 (see Figure 7 and Table 3). Moreover, NTA measurements showed the presence of particles with an average size ranging from 66 to 72 nm (a movie showing the particles can be found in supplementary information). Therefore, particles that appeared on the basolateral side were intact LNCs, with a slightly larger diameter than could be explained by some surface decoration resulting from their transcellular passage (supplementary Figure. 4S). The crossing of intact nanoparticles through the transcytosis mechanism has been already mentioned by several authors [15,42–44]. Until now, the existence of nano-objects on the basolateral side of Caco-2 monolayers has only been proven by TEM [15,45] but no evidence has been provided about their origin. More recently, Hu *et al.* [46], using confocal microscopy, did not succeed to observe any fluorescence on the basolateral side in the presence of solid lipid nanoparticles (SLNs) or simulated mixed micelles (SMMs). Working with loaded near-infrared dyes with quenching properties upon contact with water, they concluded that both SLNs and SMMs could not be transported intact across Caco-2 cell monolayers.

Table 3. FRET signal, proximity ratio, size of particles, concentration of particles (calculated with the equation obtained at 674 nm and determined by NTA) of apical and basolateral media of Caco-2 cells incubated with NEs, LNCs or HBSS for 2h at 37°C (basolateral side n=4; data are showed as mean±SD).

	<i>Time (h)</i>	<i>FRET signal</i>	<i>Proximity Ratio</i>	<i>Concentration of particles (particles/ml)</i>		<i>number average Size (nm)</i>
				<i>Calculated by fluorescence at 674 nm</i>	<i>Determined by NTA</i>	
HBSS	0 (apical side)	No	/	/	/	/
	2 (basolateral side)	No	/	/	/	/
NEs	0 (apical side)	Yes	0.549	N.A	$0.9 \cdot 10^{13}$	87.1
	2 (basolateral side)	Yes	/	/	not detected	not detected
LNCs	0 (apical side)	Yes	0.743	$6.7 \cdot 10^{12}$	$1.2 \cdot 10^{13}$	55.9
	2 (basolateral side)	No	0.748 ± 0.050	$6.2 \pm 3.8 \cdot 10^9$	$4.1 \pm 2.6 \cdot 10^9$	68.8 ± 3.0

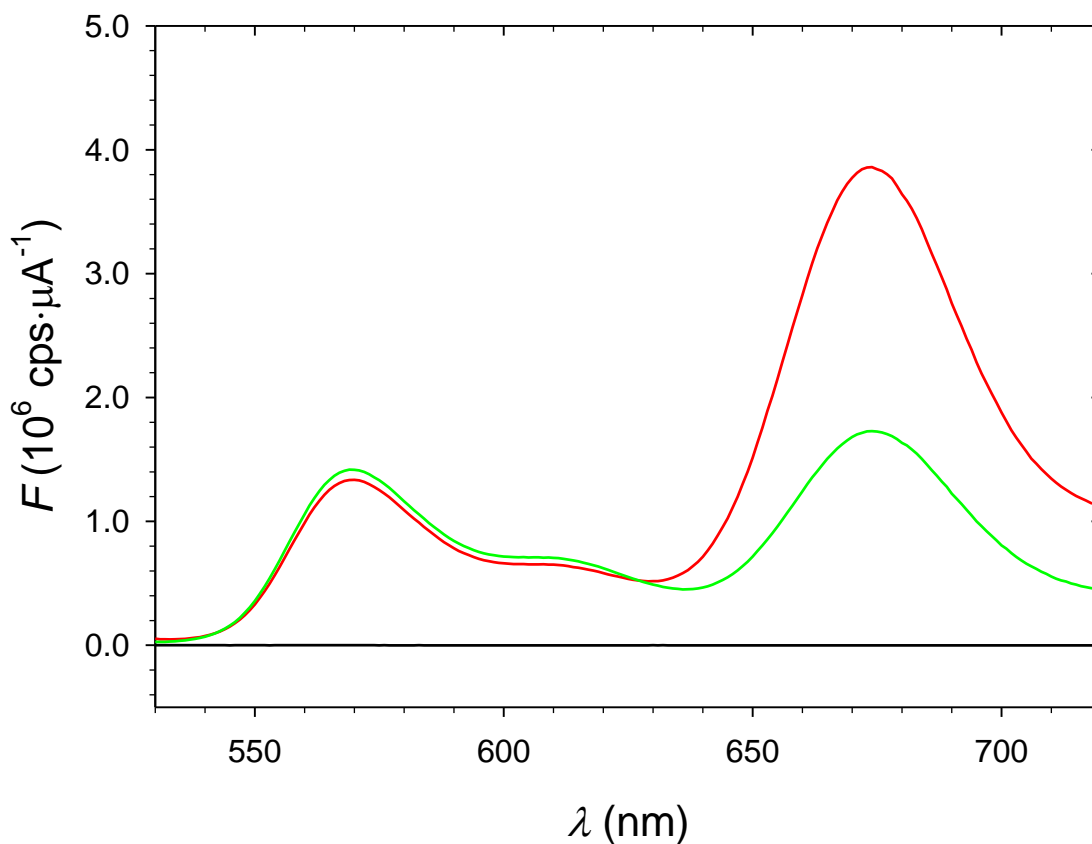


Fig. 6. Emission spectra of the apical side solution of Caco-2 cells at time zero. The black line is for an HBSS solution, the green line is for an NE solution and the red line is for an LNC solution. Emission spectra were recorded using $\lambda_{\text{ex}} = 520 \text{ nm}$ and fluorimeter settings as in Figure 4, consequently absolute intensities could be compared.

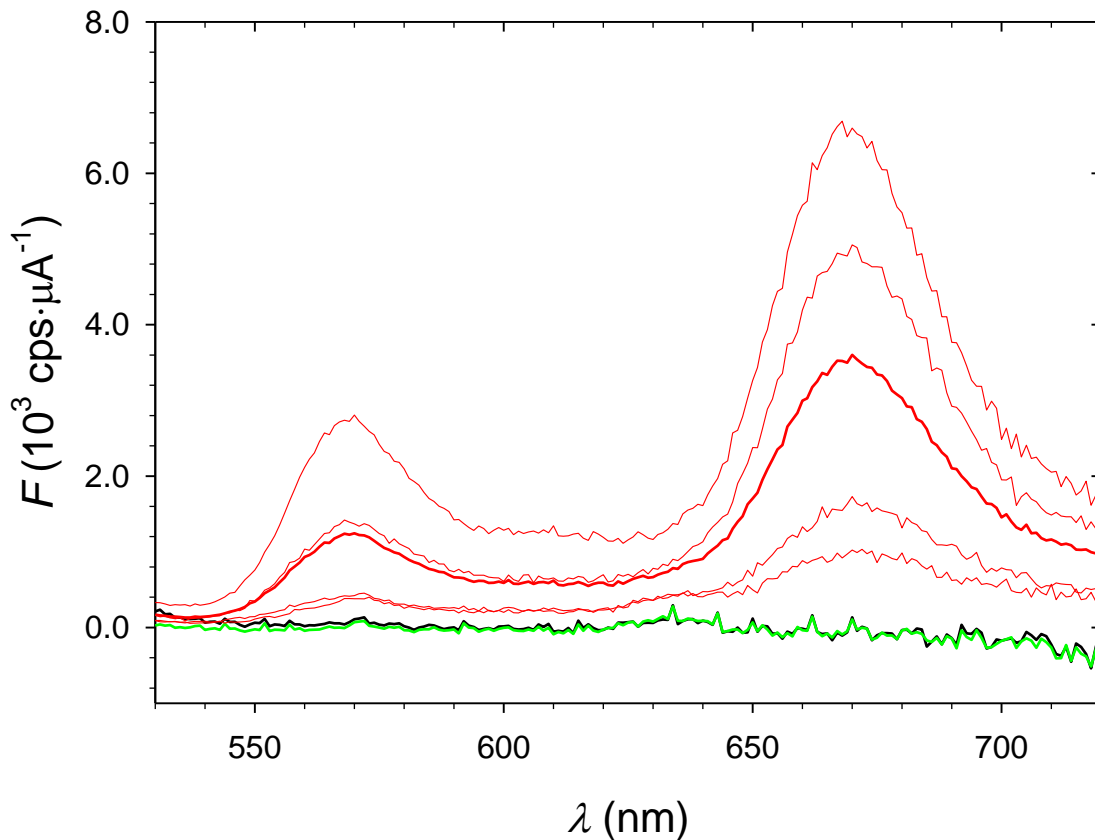


Fig. 7. Emission spectra of basolateral side solutions of Caco-2 cells after 2 hours of incubation. The black line is for an HBSS solution, the green line is for an NE solution and the thin red lines are for the 4 individual LNC trials. The bold red line represents the average response of LNC solutions. Emission spectra were recorded using $\lambda_{\text{ex}}=520$ nm and fluorimeter settings as in Figure 4, consequently absolute intensities could be compared.

Using our fluorescence calibration curve at 674 nm (acceptor wavelength) the concentration of intact FRET-LNCs on the basolateral side could be calculated and compared with NTA measurements. The average value obtained after 2h by fluorescence was $6 \pm 4 \cdot 10^9$ particles/mL and did not differ significantly from the NTA average value ($4 \pm 3 \cdot 10^9$) and fluctuations from one

well to another on were perfectly correlated. This corresponds to around 0.3% of the initial quantity of LNCs. Moreover, the same analysis has shown that $99.3 \pm 0.1\%$ ($n=4$, average $\pm S.D.$) were still on the apical side. So for the first time it was demonstrated that intact particles were transported. The low amount of transcytosis could be related to the short time exposure (only 2 hours). It should be stressed that this study was performed with the conventional Caco-2 cell model. Even if a good correlation between the *in vitro* permeability of the drug and their *in vivo* bioavailability was established [47,48], this model was not optimised for studying intestinal absorption (absence of mucus layer and M-cells or physiological medium). Moreover, the behaviour of LNCs could be affected by physico-chemical properties such as particle size, surface potential and surface functionalisation. For example, we demonstrated [15], in spite of a predominant active endocytic mechanism for the transport of LNCs, a size-dependent passive transport of LNCs (increasing with decreasing size). Moreover, better diffusion across a mucus layer of LNCs was shown with positive or neutral zeta potentials [49]. Therefore, the next step of this work will be to perform an *in vivo* study (pharmacokinetics) and assess the impact of particle surface and size.

4. Conclusions

In conclusion, very stable LNCs with high dye content, no leakage, and able to produce a very efficient FRET signal, were formulated. Using a high-sensitivity spectrofluorometer, a calibration curve down to very low LNC concentrations (less than 10^{10} particles/mL) with a FRET detection threshold even lower, was established. Fluorescence measurements were systematically supplemented by NTA experiments to measure particle sizes and concentrations. Using a Caco2 cell monolayer, it was clearly demonstrated that LNCs were able to be transported intact by transcytosis. This was not the case for FRET-NEs. LNC concentrations on

the basolateral side were successfully measured and, after 2 hours, around 0.3% of the LNCs initially present on the apical side had been transported. These unambiguous results open the way to future *in vivo* works in order to establish the pharmacokinetics and biodistribution of FRET-LNCs after their oral administration. By consequence, in a near future, standard procedures to measure the FRET signal from LNCs in blood and in relevant organs will be developed.

ACKNOWLEDGMENTS

We thank R. Bouchaala and I. Shulov for their assistance in the preparation of dye samples.

REFERENCES

- [1] G.L. Amidon, H. Lennernäs, V.P. Shah, J.R. Crison, A Theoretical Basis for a Biopharmaceutic Drug Classification: The Correlation of *in Vitro* Drug Product Dissolution and *in Vivo* Bioavailability, *Pharmaceutical Research: An Official Journal of the American Association of Pharmaceutical Scientists*. 12 (1995) 413–420. doi:10.1023/A:1016212804288.
- [2] E. Roger, F. Lagarce, E. Garcion, J.-P. Benoit, Biopharmaceutical parameters to consider in order to alter the fate of nanocarriers after oral delivery., *Nanomedicine (London, England)*. 5 (2010) 287–306. doi:10.2217/nnm.09.110.
- [3] L. Plapied, N. Duhem, A. des Rieux, V. Pr eat, Fate of polymeric nanocarriers for oral drug delivery, *Current Opinion in Colloid & Interface Science*. 16 (2011) 228–237. doi:10.1016/j.cocis.2010.12.005.
- [4] N.T. Huynh, C. Passirani, P. Saulnier, J.P. Benoit, Lipid nanocapsules: A new platform for nanomedicine, *International Journal of Pharmaceutics*. 379 (2009) 201–209.

- doi:10.1016/j.ijpharm.2009.04.026.
- [5] B. Heurtault, P. Saulnier, J.-P. Benoit, J.-E. Proust, B. Pech, J. Richard, Lipid nanocapsules, preparation method and use as medicine.WO 2001064328 A1, 2001.
- [6] B. Heurtault, P. Saulnier, B. Pech, J.-E. Proust, J.-P. Benoit, A novel phase inversion-based process for the preparation of lipid nanocarriers, *Pharmaceutical Research*. 19 (2002) 875–880. doi:10.1023/A:1016121319668.
- [7] B. Heurtault, P. Saulnier, B. Pech, M.-C. Venier-Julienne, J.-E. Proust, R. Phan-Tan-Luu, J.-P. Benoit, The influence of lipid nanocapsule composition on their size distribution, *European Journal of Pharmaceutical Sciences*. 18 (2003) 55–61. doi:10.1016/S0928-0987(02)00241-5.
- [8] S. Peltier, J.M. Oger, F. Lagarce, W. Couet, J.P. Benoit, Enhanced oral paclitaxel bioavailability after administration of paclitaxel-loaded lipid nanocapsules, *Pharmaceutical Research*. 23 (2006) 1243–1250. doi:10.1007/s11095-006-0022-2.
- [9] A.C. Groo, M. Bossiere, L. Trichard, P. Legras, J.P. Benoit, F. Lagarce, In vivo evaluation of paclitaxel-loaded lipid nanocapsules after intravenous and oral administration on resistant tumor., *Nanomedicine (London, England)*. 10 (2015) 589–601. doi:10.2217/nmm.14.124.
- [10] E. Roger, F. Lagarce, J.-P. Benoit, Development and characterization of a novel lipid nanocapsule formulation of Sn38 for oral administration., *European Journal of Pharmaceutics and Biopharmaceutics : Official Journal of Arbeitsgemeinschaft Für Pharmazeutische Verfahrenstechnik e.V.* 79 (2011) 181–8. doi:10.1016/j.ejpb.2011.01.021.
- [11] A. Ramadan, F. Lagarce, A. Tessier-Martreau, O. Thomas, P. Legras, L. Macchi, P.

- Saulnier, J.P. Benoit, Oral fondaparinux: use of lipid nanocapsules as nanocarriers and in vivo pharmacokinetic study., *International Journal of Nanomedicine*. 6 (2011) 2941–2951. doi:10.2147/IJN.S25791.
- [12] M.M. Eissa, R.M. El-Moslemany, A.A. Ramadan, E.I. Amer, M.Z. El-Azzouni, L.K. El-Khordagui, Miltefosine lipid nanocapsules for single dose oral treatment of schistosomiasis mansoni: A preclinical study, *PLoS ONE*. 10 (2015) 1–22. doi:10.1371/journal.pone.0141788.
- [13] E. Roger, F. Lagarce, J.-P. Benoit, The gastrointestinal stability of lipid nanocapsules, *International Journal of Pharmaceutics*. 379 (2009) 260–265. doi:10.1016/j.ijpharm.2009.05.069.
- [14] A.-C. Groo, P. Saulnier, J.-C. Gimel, J. Gravier, C. Ailhas, J.-P. Benoit, F. Lagarce, Fate of paclitaxel lipid nanocapsules in intestinal mucus in view of their oral delivery., *International Journal of Nanomedicine*. 8 (2013) 4291–302. doi:10.2147/IJN.S51837.
- [15] E. Roger, F. Lagarce, E. Garcion, J.-P. Benoit, Lipid nanocarriers improve paclitaxel transport throughout human intestinal epithelial cells by using vesicle-mediated transcytosis., *Journal of Controlled Release : Official Journal of the Controlled Release Society*. 140 (2009) 174–81. doi:10.1016/j.jconrel.2009.08.010.
- [16] E. Roger, F. Lagarce, E. Garcion, J.-P. Benoit, Reciprocal competition between lipid nanocapsules and P-gp for paclitaxel transport across Caco-2 cells., *European Journal of Pharmaceutical Sciences : Official Journal of the European Federation for Pharmaceutical Sciences*. 40 (2010) 422–9. doi:10.1016/j.ejps.2010.04.015.
- [17] S. Peltier, J.M. Oger, F. Lagarce, W. Couet, J.P. Benoît, Enhanced oral paclitaxel bioavailability after administration of paclitaxel-loaded lipid nanocapsules,

- Pharmaceutical Research. 23 (2006) 1243–1250. doi:10.1007/s11095-006-0022-2.
- [18] A. Niño-pariente, V.J. Nebot, M.J. Vicent, M.J. Vicent, Relevant Physicochemical Descriptors of “Soft Nanomedicines” to Bypass Biological Barriers, *Current Pharmaceutical Design*. 22 (2016) 1274–1291. doi:10.2174/1381612822666151216152143.
- [19] H. Sahoo, Forster resonance energy transfer - A spectroscopic nanoruler: Principle and applications, *Journal of Photochemistry and Photobiology C: Photochemistry Reviews*. 12 (2011) 20–30. doi:10.1016/j.jphotochemrev.2011.05.001.
- [20] R. Bouchaala, L. Mercier, B. Andreiuk, Y. Mély, T. Vandamme, N. Anton, J.G. Goetz, A.S. Klymchenko, Integrity of lipid nanocarriers in bloodstream and tumor quantified by near-infrared ratiometric FRET imaging in living mice, *Journal of Controlled Release*. 236 (2016) 57–67. doi:10.1016/j.jconrel.2016.06.027.
- [21] A.S. Klymchenko, E. Roger, N. Anton, H. Anton, I. Shulov, J. Vermot, Y. Mely, T.F. Vandamme, Highly lipophilic fluorescent dyes in nano-emulsions: towards bright non-leaking nano-droplets, *RSC Advances*. 2 (2012) 11876. doi:10.1039/c2ra21544f.
- [22] A.L. Lainé, J. Gravier, M. Henry, L. Sancey, J. Béjaud, E. Pancani, M. Wiber, I. Texier, J.L. Coll, J.P. Benoit, C. Passirani, Conventional versus stealth lipid nanoparticles: Formulation and in vivo fate prediction through FRET monitoring, *Journal of Controlled Release*. 188 (2014) 1–8. doi:10.1016/j.jconrel.2014.05.042.
- [23] J. Lu, S.C. Owen, M.S. Shoichet, Stability of self-assembled polymeric micelles in serum, *Macromolecules*. 44 (2011) 6002–6008. doi:10.1021/ma200675w.
- [24] M. Miteva, K.C. Kirkbride, K. V. Kilchrist, T.A. Werfel, H. Li, C.E. Nelson, M.K. Gupta, T.D. Giorgio, C.L. Duvall, Tuning PEGylation of mixed micelles to overcome

- intracellular and systemic siRNA delivery barriers, *Biomaterials*. 38 (2015) 97–107.
doi:10.1016/j.biomaterials.2014.10.036.
- [25] M.A. Quadir, S.W. Morton, Z.J. Deng, K.E. Shopsowitz, R.P. Murphy, T.H. Epps, P.T. Hammond, PEG – Polypeptide Block Copolymers as pH-Responsive Endosome-Solubilizing Drug Nanocarriers, *Molecular Pharmaceutics*. 11 (2014) 2420–2430.
doi:10.1021/mp500162w.
- [26] S.W. Morton, X. Zhao, M.A. Quadir, P.T. Hammond, FRET-enabled biological characterization of polymeric micelles, *Biomaterials*. 35 (2014) 3489–3496.
doi:10.1016/j.biomaterials.2014.01.027.
- [27] J. Gravier, L. Sancey, S. Hirsjärvi, E. Rustique, C. Passirani, J.P. Benoit, J.L. Coll, I. Texier, FRET imaging approaches for in vitro and in vivo characterization of synthetic lipid nanoparticles, *Molecular Pharmaceutics*. 11 (2014) 3133–3144.
doi:10.1021/mp500329z.
- [28] S. Lee, J.Y. Tyler, S. Kim, K. Park, J. Cheng, FRET imaging reveals different cellular entry routes of self-assembled and disulfide bonded polymeric micelles, *Molecular Pharmaceutics*. 10 (2013) 3497–3506. doi:10.1021/mp4003333.
- [29] H.T.P. Nguyen, E. Allard-Vannier, C. Gaillard, I. Eddaoudi, L. Miloudi, M. Soucé, I. Chourpa, E. Munnier, On the interaction of alginate-based core-shell nanocarriers with keratinocytes in vitro, *Colloids and Surfaces B: Biointerfaces*. 142 (2016) 272–280.
doi:10.1016/j.colsurfb.2016.02.055.
- [30] K.Y. Lu, C.W. Lin, C.H. Hsu, Y.C. Ho, E.Y. Chuang, H.W. Sung, F.L. Mi, FRET-based dual-emission and pH-responsive nanocarriers for enhanced delivery of protein across intestinal epithelial cell barrier, *ACS Applied Materials and Interfaces*. 6 (2014) 18275–

18289. doi:10.1021/am505441p.
- [31] H. Li, M. Chen, Z. Su, M. Sun, Q. Ping, Size-exclusive effect of nanostructured lipid carriers on oral drug delivery, *International Journal of Pharmaceutics*. 511 (2016) 524–537. doi:10.1016/j.ijpharm.2016.07.049.
- [32] S. Preus, L.M. Wilhelmsson, Advances in Quantitative FRET-Based Methods for Studying Nucleic Acids, *ChemBioChem*. 13 (2012) 1990–2001. doi:10.1002/cbic.201200400.
- [33] G. Bastiat, C.O. Pritz, C. Roider, F. Fouchet, E. Lignières, A. Jesacher, R. Glueckert, M. Ritsch-Marte, A. Schrott-Fischer, P. Saulnier, J.P. Benoit, A new tool to ensure the fluorescent dye labeling stability of nanocarriers: A real challenge for fluorescence imaging, *Journal of Controlled Release*. 170 (2013) 334–342. doi:10.1016/j.jconrel.2013.06.014.
- [34] V.N. Kilin, H. Anton, N. Anton, E. Steed, J. Vermot, T.F. Vandamme, Y. Mely, A.S. Klymchenko, Counterion-enhanced cyanine dye loading into lipid nano-droplets for single-particle tracking in zebrafish, *Biomaterials*. 35 (2014) 4950–4957. doi:10.1016/j.biomaterials.2014.02.053.
- [35] P. Artursson, K. Palm, K. Luthman, Caco-2 monolayers in experimental and theoretical predictions of drug transport, *Advanced Drug Delivery Reviews*. 64 (2012) 280–289. doi:10.1016/j.addr.2012.09.005.
- [36] P. Balimane, S. Chong, A critique of cell culture models for intestinal permeability., *Drug Discovery Today*. 10 (2005) 335–343. doi:10.1016/S1359-6446(04)03354-9.
- [37] N. Anton, T.F. Vandamme, The universality of low-energy nano-emulsification, *International Journal of Pharmaceutics*. 377 (2009) 142–147.

- doi:10.1016/j.ijpharm.2009.05.014.
- [38] N. Anton, J.P. Benoit, P. Saulnier, Design and production of nanoparticles formulated from nano-emulsion templates-A review, *Journal of Controlled Release*. 128 (2008) 185–199. doi:10.1016/j.jconrel.2008.02.007.
- [39] N. Anton, P. Gayet, J.-P. Benoit, P. Saulnier, Nano-emulsions and nanocapsules by the PIT method: An investigation on the role of the temperature cycling on the emulsion phase inversion, *International Journal of Pharmaceutics*. 344 (2007) 44–52. doi:http://dx.doi.org/10.1016/j.ijpharm.2007.04.027.
- [40] C. Simonsson, G. Bastiat, M. Pitorre, A.S. Klymchenko, J. Béjaud, Y. Mély, J.P. Benoit, Inter-nanocarrier and nanocarrier-to-cell transfer assays demonstrate the risk of an immediate unloading of dye from labeled lipid nanocapsules, *European Journal of Pharmaceutics and Biopharmaceutics*. 98 (2016) 47–56. doi:10.1016/j.ejpb.2015.10.011.
- [41] B.K. Müller, E. Zaychikov, C. Bräuchle, D.C. Lamb, Pulsed interleaved excitation., *Biophysical Journal*. 89 (2005) 3508–22. doi:10.1529/biophysj.105.064766.
- [42] M.S. Cartiera, K.M. Johnson, V. Rajendran, M.J. Caplan, W.M. Saltzman, The uptake and intracellular fate of PLGA nanoparticles in epithelial cells, *Biomaterials*. 30 (2009) 2790–2798. doi:10.1016/j.biomaterials.2009.01.057.
- [43] A. Beloqui, M.Á. Solinís, A.R. Gascón, A. Del Pozo-Rodríguez, A. Des Rieux, V. Prétat, Mechanism of transport of saquinavir-loaded nanostructured lipid carriers across the intestinal barrier, *Journal of Controlled Release*. 166 (2013) 115–123. doi:10.1016/j.jconrel.2012.12.021.
- [44] Z. Zhang, H. Bu, Z. Gao, Y. Huang, F. Gao, Y. Li, The characteristics and mechanism of simvastatin loaded lipid nanoparticles to increase oral bioavailability in rats, *International*

- Journal of Pharmaceutics. 394 (2010) 147–153. doi:10.1016/j.ijpharm.2010.04.039.
- [45] W. Du, Y. Fan, N. Zheng, B. He, L. Yuan, H. Zhang, X. Wang, J. Wang, X. Zhang, Q. Zhang, Transferrin receptor specific nanocarriers conjugated with functional 7peptide for oral drug delivery, *Biomaterials*. 34 (2013) 794–806. doi:10.1016/j.biomaterials.2012.10.003.
- [46] X. Hu, W. Fan, Z. Yu, Y. Lu, J. Qi, J. Zhang, X. Dong, W. Zhao, W. Wu, Evidence does not support absorption of intact solid lipid nanoparticles via oral delivery., *Nanoscale*. 8 (2016) 7024–35. doi:10.1039/c5nr07474f.
- [47] H. Lennernas, K. Palm, U. Fagerholm, P. Artursson, Comparison between active and passive drug transport in human intestinal epithelial (Caco-2) cells in vitro and human jejunum in vivo, *Int J Pharm [0378-5173]*. 127 (1996) 103–107.
- [48] H. Le-Thi-Thu, Y. Canizares-Carmenate, Y. Marrero-Ponce, F. Torrens, J. A. Castillo-Garit, Prediction of Caco-2 Cell Permeability Using Bilinear Indices and Multiple Linear Regression, *Letters in Drug Design & Discovery*. 13 (2015) 161–169. doi:10.2174/1570180812666150630183511.
- [49] A.-C. Groo, K. Mircheva, J. Bejaud, C. Ailhas, I. Panaiotov, P. Saulnier, T. Ivanova, F. Lagarce, Development of 2D and 3D mucus models and their interactions with mucus-penetrating paclitaxel-loaded lipid nanocapsules., *Pharmaceutical Research*. 31 (2014) 1753–65. doi:10.1007/s11095-013-1280-4.

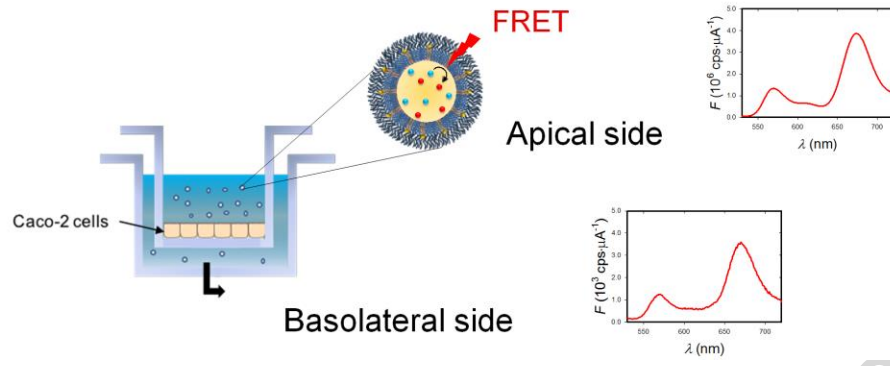
SUPPORTING DATA

Additional figures (fluorescent spectra, a calibration curve and number distribution of particles) (PDF)

VIDEO

A Movies showing the motion of nanoparticles (AVI)

ACCEPTED MANUSCRIPT



Graphical abstract

ACCEPTED MANUSCRIPT